Pflugers Arch - Eur J Physiol (2012) 464:249–259
DOI 10.1007/s00424-012-1133-8

ION CHANNELS, RECEPTORS AND TRANSPORTERS

Regulation of Cx45 hemichannels mediated by extracellular and intracellular calcium

Patrick Bader · Robert Weingart · Marcel Egger

Received: 15 March 2012 / Revised: 13 June 2012 / Accepted: 15 June 2012 / Published online: 26 June 2012

Abstract Connexin45 (Cx45) hemichannels (HCs) open in the absence of Ca^{2+} and close in its presence. To elucidate the underlying mechanisms, we examined the role of extra- and intracellular Ca^{2+} on the electrical properties of HCs. Experiments were performed on HeLa cells expressing Cx45 using electrical (voltage clamp) and optical (Ca^{2+} imaging) methods. HCs exhibit a time- and voltage-dependent current (I_{hc}), activating with depolarization and inactivating with hyperpolarization. Elevation of $[Ca^{2+}]_o$ from 20 nM to 2 μM reversibly decreases I_{hc}, decelerates its rate of activation, and accelerates its deactivation. Our data suggest that $[Ca^{2+}]_o$ modifies the channel properties by adhering to anionic sites in the channel lumen and/or its outer vestibule. In this way, it blocks the channel pore and reversibly lowers I_{hc} and modifies its kinetics. Rapid lowering of $[Ca^{2+}]_o$ from 2 mM to 20 nM, achieved early during a depolarizing pulse, led to an outward I_{hc} that developed with virtually no delay and grew exponentially in time paralleled by unaffected $[Ca^{2+}]_i$. A step increase of $[Ca^{2+}]_i$ evoked by photorelease of Ca^{2+} early during a depolarizing pulse led to a transient decrease of I_{hc} superimposed on a growing outward I_{hc}; a step decrease of $[Ca^{2+}]_i$ elicited by photoactivation of a Ca^{2+} scavenger provoked a transient increase in I_{hc}. Hence, it is tempting to assume that Ca^{2+} exerts a direct effect on Cx45 hemichannels.

P. Bader · R. Weingart · M. Egger (✉)
Department of Physiology, University of Bern,
Bühlplatz 5,
3012 Bern, Switzerland
e-mail: egger@pyl.unibe.ch

Present Address:
P. Bader
Department of Molecular and Cellular Physiology,
Beckman Center, Stanford University,
B105, 279 Campus Drive,
Stanford, CA 94305, USA

Keywords Gap junction hemichannel · Electrical properties · Calcium · Connexin45

Introduction

Gap junction channels (GJC) and hemichannels (HC) are regulated by different means, including electrical gating, chemical gating, and biochemical modulation. The underlying mechanisms involve voltage gradient, intra-/extracellular ions and lipophilic molecules, or phosphorylation [6, 17, 44]. The availability of convenient methods to measure small currents may have led to the impression that voltage gating is the most biologically important mechanism. However, in most tissues and under a variety of situations, chemical gating and biochemical modulation are presumably more important and Ca^{2+} seems to be substantially involved in these regulatory functions.

Since nearly four decades ago, it was reported that Ca^{2+} is causally involved in the process of "healing over" in cardiac tissue [8]. This phenomenon is based on Ca^{2+} entry into damaged cardiac cells followed by closing of GJCs. Intact tissue is consequently isolated from damaged cells, thus re-establishing the integrity of the syncytial tissue. This pivotal result initiated a research area focused on chemical regulation of GJCs [20]. It has since been shown that intracellular Ca^{2+} exerts conflicting effects on GJCs: at elevated $[Ca^{2+}]_i$ (>500 nM), it closes channels and prevents functional cell–cell interactions [e.g., 21, 25, 32, 45]; at physiological $[Ca^{2+}]_i$ (~100 nM), it diffuses through open channels and assists propagation of intercellular Ca^{2+} waves, thus acting as second messenger [27].

The current concept is based on the assumption that GJCs consist of paired HCs arranged in series, and that each HC accommodates two separate voltage-sensitive gating mechanisms [6]. One mechanism, termed fast V_j gating, describes

the sensitivity to the voltage between the cells of a pair, i.e., the transjunctional voltage V_j. The other mechanism is termed slow V_j gating or "loop gating" because it resembles the gating transitions during the initial opening of newly formed GJCs [5, 38]. It is fairly well established that unpaired HCs are precursors of GJCs and also exert functional roles on their own [33]. While GJCs in the cell–cell configuration are open in most situations and form a cytoplasmic continuum, unopposed HCs in single cells are usually closed. When open, they connect the cell interior with the extracellular space. Because HCs have large poorly selective pores, they accommodate not only ions but also molecules up to 1.2 kDa, including metabolites and signaling molecules. Unregulated flow through the channels would therefore cause cells to readily lose their contents and perish. However, if HC openings were brief, i.e., when controlled by gating mechanisms, they could provide a pathway for release (or uptake) of signaling molecules and ions. Indeed, such tasks have been ascribed to HCs in multiple cell types and associated with diverse functions [9, 14, 29, 34, 46]. These studies propose a signaling pathway involving propagated intercellular Ca^{2+} waves, mediated by HC-dependent ATP release and subsequent activation of purinergic receptors in neighboring cells. Single cells expressing HCs have also been used to examine properties of GJCs that are not directly accessible to studies on GJCs in cell pair experiments [28].

In this study, we have examined the effects of Ca^{2+} on the properties of Cx45 HCs expressed in HeLa cells. This connexin (Cx) is prominently expressed in heart [30], blood vessels [16], neurons [26], and retina [31], and thus may control diverse biological processes. We found that Ca^{2+} exerts a direct effect on Cx45 hemichannels. This regulatory mechanism is consistent with the view that external Ca^{2+} can modify HC properties by reversible binding to regulatory sites located in the channel lumen and/or its outer vestibule, thus affecting voltage sensors and blocking/unblocking the pore.

Methods

Cells and solutions

Transfected human HeLa cells expressing mouse Cx45 (GJC1; see www.genenames.org/genefamily/gj.php) and non-transfected HeLa cells (both kindly provided by K. Willecke, Bonn, Germany [7, 12]) were grown in Dulbecco's medium (DMEM) containing 10 % fetal calf serum (FCS), 100 μg/ml streptomycin, and 100 U/ml penicillin. Transfected cells were selected with 0.5–1 μM puromycin. To perform experiments, the cells were harvested in DMEM with 10 % FCS (0.2×10^6 to 1×10^6 cells/ml), seeded onto sterile glass coverslips placed in multiwell culture dishes, and used within 1–2 days.

Experiments were carried out in K^+-rich solution with normal Ca^{2+} (mM): KCl 140, NaCl 4, $CaCl_2$ 2, $MgCl_2$ 1, HEPES 5 (pH 7.4), glucose 5, pyruvate 2, $CsCl_2$ 2, $BaCl_2$ 1, TEA-Cl 2, or with reduced Ca^{2+} (mM): EGTA 10; $CaCl_2$ was added to adjust the free $[Ca^{2+}]_o$ to 20 nM (pCa 7.7) using Patcher's Power Tools (IgorPro Tool Collection; F. Mendez and F. Würiehausen, MPI, Göttingen, Germany). Solutions with intermediate free $[Ca^{2+}]_o$ were obtained by adding appropriate amounts of $CaCl_2$. Patch pipettes were filled with normal pipette solution (mM): KCl 140, NaCl 4, $CaCl_2$ 1, $MgCl_2$ 1, Mg-ATP 3, HEPES 5 (pH 7.2), EGTA 5 (free $[Ca^{2+}]_i$ 40 nM, pCa 7.4), $CsCl_2$ 2, $BaCl_2$ 1, and TEA-Cl 2, filtered through 0.2-μm pores. Ba^{2+}, Cs^+, and TEA^+ served to block K^+ channels and hence increase the input resistance. Extracellular solutions were complemented with 40 μM Mibefradil (gift from Roche Pharma, Basel, Switzerland) to block the volume-regulated anion channels [1, 2]. All solutions were adjusted to 310 mOsm by adding mannitol. The bath solution was exchanged by means of a gravity system.

Measurement of hemichannel currents

Glass coverslips with adherent cells were transferred to an experimental chamber superfused with saline at room temperature (22–25 °C) and mounted on an inverted microscope (Diaphot-TMD, Nikon; Nippon Kogaku, Tokyo, Japan). Patch pipettes were pulled from glass capillaries (GC150F-10; Harvard Apparatus, Edenbridge, UK) by means of a horizontal puller (DMZ-Universal; Zeitz Instruments, Munich, Germany). To reduce the capacitance, the tip of the pipettes was coated with a silicon elastomer (Sylgard 184; Dow Corning, Wiesbaden, Germany). Filled with solution, the pipettes had a DC resistance of 2–6 MΩ. Pipettes were fixed in a holder mounted on a micromanipulator (MP-258; Sutter Instrument, Novato, CA, USA) and connected to an amplifier (EPC 7; HEKA Elektronik, Darmstadt, Germany). Single cells were voltage clamped in the whole-cell configuration of the patch-clamp technique [1]. For analysis, the signals were filtered at 1 kHz (eight-pole Bessel filter) and digitized at 3 kHz with an A/D converter (ITC-16; Instrutech, Port Washington, NY, USA). Data acquisition and analysis were done with Pulse/PulseFit software (HEKA Elektronik). Curve fitting and statistical analysis were performed with SigmaPlot and SigmaStat, respectively (Jandel Scientific, Erkrath, Germany). The results are presented as means ±1 SEM ($p\leq0.05$ was considered significant). Given p values are calculated using a t statistics.

Current recording combined with confocal microscopy and UV-flash photolysis

Internal solution contained (mM): KCl 144, HEPES 5, CsCl 2, $BaCl_2$ 1, TEA-Cl 2, K_2-ATP 5, fluo-3-K 0.1, reduced glutathione (GSH) 2, Na_4-DM-nitrophen 2 (unphotolyzed K_D for Ca^{2+} 80 nM), or K_4-diazo-2 (unphotolyzed K_D for Ca^{2+} 2.2 μM); $CaCl_2$ was added to adjust the free $[Ca^{2+}]_i$ to 100 nM using Patcher's Power Tools, pH 7.2 (KOH); external solution contained (mM): KCl 144, HEPES 5, CsCl 2, $BaCl_2$ 1, TEA-Cl 2, $MgCl_2$ 1, Pyruvat 2, Glucose 5, EGTA 5, and mibefradil 40 μM, pH 7.4 (KOH), adjusted to 310 mOsm (see above). Where required, the superfusion solution contained 2 mM $CaCl_2$ instead of EGTA. Rapid changes of the extracellular solutions were performed with a gravity-driven superfusion system ($t_{1/2}\approx$ 400 ms). The Ca^{2+} pump of endoplasmic reticulum was blocked adding 0.1 μM thapsigargin (Alomone Labs, Jerusalem, Israel) to the bath solution. The interference with the Na^+/Ca^{2+} exchanger can be assumed as negligible. This was verified in the presence of 8 or 1 mM Ni^{2+} in the bath solution (data not shown).

Membrane currents were recorded with an Axopatch 200 voltage-clamp amplifier (Axon Instruments, Foster City, CA, USA). Data were acquired using custom-written software developed under LabView software (National Instruments, Ennetbaden, Switzerland). Data analysis was carried out with IgorPro software (WaveMetrics, Lake Oswego, OR, USA).

The Ca^{2+} indicator fluo-3 (Biotium, Hayward, CA, USA) was excited with the 488 nm line of an argon-ion laser (Model 5000; Ion Laser Technology, Salt Lake City, NE, USA) at 50 μW intensity on the cell. The fluorescence was detected at 540±15 nm with a confocal laser-scanning microscope operated in the line-scan mode (MRC 1000; Bio-Rad, Hemel Hempstead, UK). Amplitude and time course of $[Ca^{2+}]_i$ are shown as fluo-3 self-ratios (F/F_0). Ultraviolet-light flashes (wavelength 340–390 nm, flash duration 400 μs, discharged energy 230 J) were used to photolyze intracellular DM-nitrophen (Calbiochem, VWR, Dietikon, Switzerland) or diazo-2 (Molecular Probes, Eugene OR, USA) in an epi-illumination arrangement and were generated with a xenon short-arc flash lamp. The UV light was coupled into the microscope via an optical light guide. After reflection at a dichroic mirror, the light passed through the microscope objective (Neofluar ×63, NA 1.25; Zeiss) generating a homogeneous illumination of the entire visible field. All experiments were carried out at room temperature (20–22 °C).

Results

Effects of extracellular Ca^{2+} on hemichannel currents

Under physiological conditions, single HCs are usually closed. However, as previously shown, they can be forced to open by reduced extracellular Ca^{2+} [1, 39]. To further study this behavior, we have examined the effects of different $[Ca^{2+}]_o$ on currents carried by HCs in transfected HeLa cells expressing Cx45.

Figure 1, upper panel, illustrates the pulse protocol. Superimposed on a holding potential V_h=0 mV, a dual voltage pulse was administered every 30 s. It consisted of a conditioning pulse to 50 mV for 6 s followed by a test pulse to −50 mV for 3 s. Since the major charge carriers were set to $[K^+]_o = [K^+]_i$ (see "Methods"), the net charge transfer at V_h=0 mV was minimal. Figure 1, lower panel, shows superimposed HC currents, I_{hc}, from a cell consecutively exposed to bath solutions containing 20 nM (large signal), 2 μM (medium signal), and 2 mM $[Ca^{2+}]_o$ (small signal), i.e., control condition. In both solutions with reduced $[Ca^{2+}]_o$, depolarization of the membrane potential, V_m, gave rise to an outward current consisting of a rapid initial rise followed by a time-dependent increase, and hyperpolarization caused an inward current that decayed with time. Hence, I_{hc} was activated on depolarization and deactivated on hyperpolarization. The reversal potential of the HCs turned out to be ~0 mV. In solution with $[Ca^{2+}]_o$= 2 mM, the pulse protocol elicited a marginal outward current of constant amplitude followed by a small inward current with a hint of a decay due to suboptimal solution change and/or unspecified background currents. Under optimal conditions, no time-dependent current was discernable [1, 39]. Moreover, as reported before, wild-type HeLa cells yielded no extra current in low $[Ca^{2+}]_o$, implying that the extra currents in Fig. 1 are carried by Cx45 HCs [1, 39].

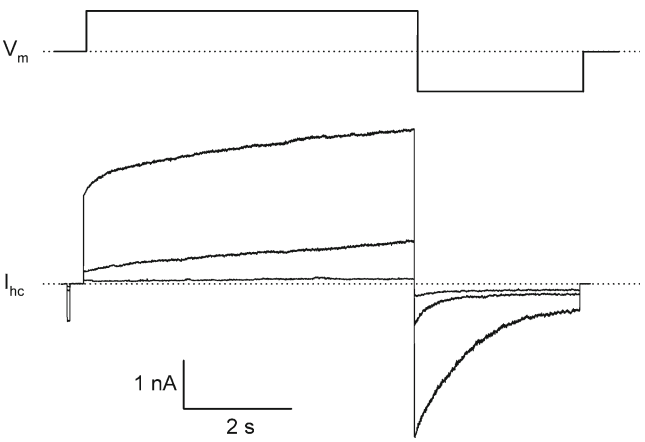

Fig. 1 **a**, **b** Role of extracellular Ca^{2+} on HC currents, I_{hc}. **a** Voltage-clamp protocol with a conditioning pulse to 50 mV for 6 s followed by a test pulse to −50 mV for 3 s. Holding potential V_h=0 mV. **b** Superimposed traces I_{hc} recorded in solution with 20 nM (large signal), 2 μM (medium size signal), and 2 mM $[Ca^{2+}]_o$ (small signal). I_{hc} at the end of the conditioning pulse corresponds to $I_{hc,max}$ (max—maximal); I_{hc} at the beginning and end of the test pulse correspond to $I_{hc,inst}$ (inst—instantaneous), and $I_{hc,ss}$ (ss—steady state), respectively. Lowering of $[Ca^{2+}]_o$ enhances $I_{hc,max}$, $I_{hc,inst}$, and $I_{hc,ss}$

To further explore the effects of $[Ca^{2+}]_o$ on the properties of I_{hc}, the amplitude of the test pulse was altered in steps of 20 mV between V_m=±50 mV, while the amplitude of the conditioning pulse was maintained to reassure that the activation of I_{hc} was kept constant. The associated I_{hc} signals were recorded for analysis. To get an estimate of the responses, control solution ($[Ca^{2+}]_o$=2 mM) in the bath was replaced by test solution with 20 nM free Ca^{2+}. Thereafter, $[Ca^{2+}]_o$ was elevated by superfusion with test solutions containing 200 nM or 2 μM free Ca^{2+}.

Each I_{hc} recording of a cell was analyzed in terms of the amplitude at the beginning and end of a test pulse to yield a value for $I_{hc,inst}$ (inst—instantaneous) and $I_{hc,ss}$ (ss—steady state) and to calculate the respective conductances $g_{hc,inst}$ and $g_{hc,ss}$. The $g_{hc,inst}$ data of each cell were scaled by referring to a value extrapolated to V_m= 0 mV; scaling of $g_{hc,ss}$ data involved expression as a fraction of $g_{hc,inst}$ on a pulse-to-pulse basis [1]. The scaled $g_{hc,ss}$ data obtained in solutions of different $[Ca^{2+}]_o$ were then normalized to the maximal $g_{hc,ss}$ at V_m=50 mV in the presence of 20 nM $[Ca^{2+}]_o$. The normalized $g_{hc,ss}$ data from individual cells were sampled, averaged, and plotted as a function of V_m.

Figure 2a shows the graphs for the solutions with $[Ca^{2+}]_o$= 20 nM (filled circles), 200 nM (open circles), and 2 μM (open squares). For each $[Ca^{2+}]_o$ examined, the normalized relationship between $g_{hc,ss}$ and V_m was sigmoidal with a minimum at negative V_m, i.e., $g_{hc,min}$, and a maximum at positive V_m, i.e., $g_{hc,max}$, thus exhibiting a positive slope. In the presence of $[Ca^{2+}]_o$=20 nM, the lowest concentration tested, the values of $g_{hc,ss}$ were largest. As $[Ca^{2+}]_o$ was increased, the values of $g_{hc,max}$ and $g_{hc,min}$ decreased. Hence, elevation of $[Ca^{2+}]_o$ provoked a decrease in $g_{hc,ss}$ over the entire voltage range examined, thus compressing the amplitude of the function $g_{hc,ss} = f(V_m)$. These findings indicate that $[Ca^{2+}]_o$ and $g_{hc,ss}$ are inversely proportional. Note that $g_{hc,ss}$ failed to reach zero at large negative voltage.

The normalized $g_{hc,ss}$ data gained at $[Ca^{2+}]_o$=20 nM, 200 nM, and 2 μM were fitted to the Boltzmann equation assuming a two-state process:

$$\frac{g_{hc,ss}}{g_{hc,inst}} = \frac{g_{hc,max} - g_{hc,min}}{1 + e^{\left[A\left(V_m - V_{m,0}\right)\right]}} + g_{hc,min}. \quad (1)$$

$V_{m,0}$ corresponds to V_m at which $g_{hc,ss}$ is half-maximally activated; A is a constant expressing gating charge $zq(kT)^{-1}$ (z = unitary positive charge q moving through the electric field applied; k = Boltzmann constant; T = Kelvin temperature; cf. Harris et al. [17]). The smooth curves in Fig. 2a represent the best fit of data to Eq. (1) for $[Ca^{2+}]_o$=20 nM (continuous curve), 200 nM (dashed curve), and 2 μM (pointed curve). Table 1 summarizes the Boltzmann parameters obtained. They indicate that $[Ca^{2+}]_o$ affected $g_{hc,max}$ and $g_{hc,min}$, thus altering the apparent steepness of the sigmoidal curves, characterized by z.

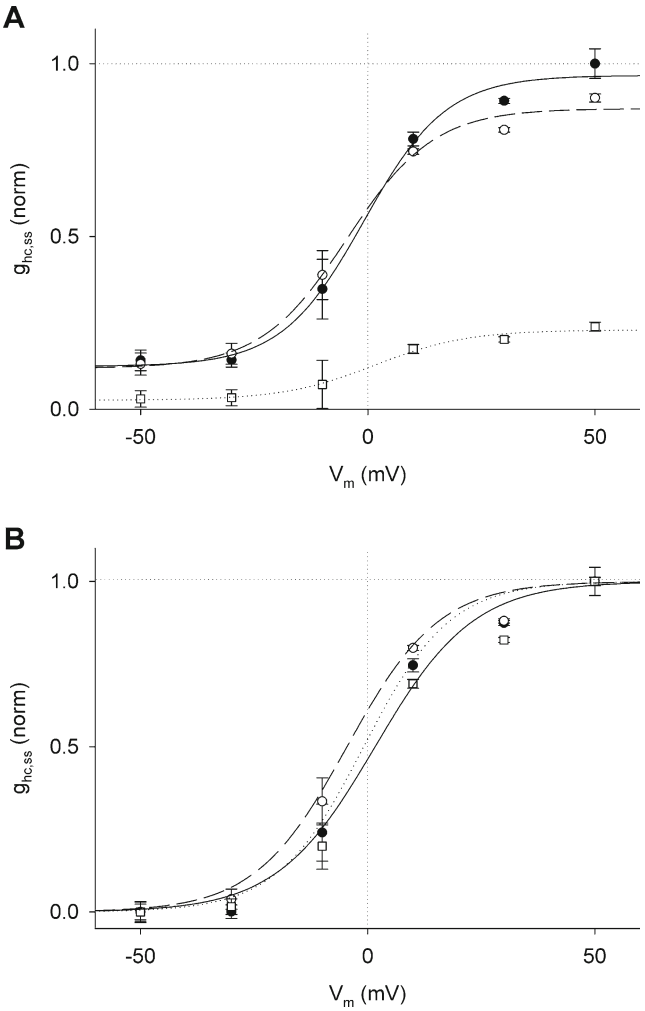

Fig. 2 **a**, **b** Effects of different $[Ca^{2+}]_o$ on the relationship between $g_{hc,ss}$ (HC conductance at steady state) and V_m (membrane potential). Currents were elicited by the dual-pulse protocol with a constant conditioning pulse (50 mV, 6 s) and a variable test pulse (range, ±50 mV, 20 mV steps, 3 s). **a** Plots of normalized $g_{hc,ss}$ as a function of V_m obtained at different $[Ca^{2+}]_o$: 20 nM (*filled circles*; solid curve), 200 nM (*open circles*; dashed curve), and 2 μM (*open squares*; pointed curve). They emphasize the differences in $g_{hc,ss}$ amplitude. *Symbols* represent means ±1 SEM calculated from six to nine cells. The curves correspond to the best fit of data to the Boltzmann equation (for values, see Table 1). **b** Replots of $g_{hc,ss}$ data emphasizing the voltage sensitivity of $g_{hc,ss}$. The fitted curves $g_{hc,ss} = f(V_m)$ shown in panel (**a**) were transformed to vary between $g_{hc,min}$=0 and $g_{hc,max}$=1, thus representing the voltage-sensitive part of $g_{hc,ss}$. The curves are the best fit to the Boltzmann equation (for parameters, see text). They are nearly superimposed implying that $[Ca^{2+}]_o$ did not affect the voltage sensitivity of $g_{hc,ss}$

The graph in Fig. 2b repeats the data of Fig. 2a in a format that allows a direct comparison of the voltage sensitivity of the different $g_{hc,ss}$ curves. To this end, the fitted curve $g_{hc,ss}=f(V_m)$ at each $[Ca^{2+}]_o$ was transformed to vary from $g_{hc,min}$=0 to $g_{hc,max}$=1, to emphasize the voltage-sensitive span of $g_{hc,ss}$. The resulting

Table 1 Effects of external Ca^{2+} on gating properties of Cx45 HCs

$[Ca^{2+}]_o$	$V_{m,0}$ (mV)	$g_{hc,min}$	$g_{hc,max}$	z
20 nM	−0.85	0.12	0.97	2.81
200 nM	−4.53	0.12	0.87	2.68
2 μM	1.64	0.03	0.23	2.53

Boltzmann parameters: $V_{m,0}$: V_m at which $g_{hc,ss}$ is half-maximally deactivated; $g_{hc,min}$: minimal conductance at large negative V_m; $g_{hc,max}$: maximum conductance at large positive V_m; z: equivalent number of unitary positive charges q moving through the electric field applied. For explanations, see text

curves are nearly superimposed (symbols in Fig. 2a and b are identical). They are best described by the following Boltzmann parameters, $V_{m,0}$ and z: $[Ca^{2+}]_o$= 20 nM: −0.94 mV and −2.65; $[Ca^{2+}]_o$=200 nM: −2.77 mV and −2.48; $[Ca^{2+}]_o$=2 μM: 3.79 mV and −2.32. These data indicate that $[Ca^{2+}]_o$ does not significantly shift the function $g_{hc,ss} = f(V_m)$ along the voltage axis.

The current recordings in Fig. 1 and others from the same set of experiments have also been used to study the role of external Ca^{2+} on the kinetic properties of I_{hc}. Depolarization of V_m to 50 mV led to an outward current with a sudden rise, $I_{hc,inst}$, followed by a time-dependent increase, and hyperpolarization to −50 mV caused an inward current decaying with time. Both the size and the contour of I_{hc} was sensitive to external $[Ca^{2+}]_o$. With regard to size, elevation of Ca^{2+} from 20 nM to 2 μM gave rise to a decrease in amplitude of both components of outward current and a decrease in amplitude of inward current. Such elevations of $[Ca^{2+}]$ also slowed down the time-dependent increase of I_{hc} during depolarization and sped up its time-dependent decrease during hyperpolarization.

To determine kinetic properties, the I_{hc} records were treated with a least-square curve-fitting procedure [1]. Upon depolarization, I_{hc} increased with time as sum of two exponentials providing two time constants of activation, τ_{a1} and τ_{a2}; upon hyperpolarization, it decreased as a single exponential entailing a single time constant of deactivation, τ_d. Table 2 summarizes the averaged time constants. In the case of I_{hc} activation, the analysis also furnished values of the fractional amplitudes of I_{hc} at steady state, C_1 and C_2, reflecting the relative contribution of both activation processes.

Figure 3 shows the concentration–response relationship documenting the effect of $[Ca^{2+}]_o$ on $g_{hc,max}$. It includes data obtained at $[Ca^{2+}]_o$=20 nM (n=20), 200 nM (n=10), 2 μM (n=15), 20 μM (n=5), 200 μM (n=7), and 2 mM (n=10). The normalized $g_{hc,ss}$ values at V_m=50 mV, i.e., $g_{hc,max}$, were plotted as a function of the negative logarithm of $[Ca^{2+}]_o$, i.e., pCa_o. The symbols represent mean values ±1 SEM (filled circles). The solid curve is the best fit of data to the sum of two Hill equations:

$$g_{hc,max}(\text{norm}) = a_1 \frac{1}{1 + \left(K_{1Ca}/[Ca^{2+}]_o\right)^{n_1}} + a_2 \frac{1}{1 + \left(K_{2Ca}/[Ca^{2+}]_o\right)^{n_2}}. \quad (2)$$

It was obtained assuming two separate processes with a relative contribution of a_1=0.85 and a_2=0.15 (p<0.0001) for $g_{hc,max}(\text{norm})_1$ and $g_{hc,max}(\text{norm})_2$ at steady state, respectively. The Hill parameters were pK'_{1Ca}=6.18 and pK'_{2Ca}= 3.67 [apparent binding constants, corresponding to K_{1Ca}= 0.66 μM (p<0.0001) and K_{2Ca}=216 μM (p<0.003), respectively]; n_1=2.1 (p<0.0001) and n_2=5.1 (p<0.8) (Hill coefficient). The values of n place a lower limit of two and five Ca^{2+} binding sites per HC.

Response time of hemichannel currents to rapid changes in $[Ca^{2+}]_o$

A set of experiments was carried out to study the response time of I_{hc} to rapid changes in $[Ca^{2+}]_o$. As shown in Fig. 4, I_{hc} was elicited by means of a dual-voltage pulse with the conditioning pulse set to 30 mV for 15 s and the test pulse to −40 mV for 3 s (trace A). Early during the conditioning pulse, $[Ca^{2+}]_o$ in the proximity of the cell was rapidly changed ($t_{0.5}$≈0.4 s) from 2 mM to 20 nM (trace D). This provoked a prominent outward current that activated exponentially with time (trace B). It was initiated quasi-simultaneously

Table 2 Effects of external Ca^{2+} on kinetic properties of Cx45 HC currents, I_{hc}

$[Ca^{2+}]_o$	τ_{a1} (s)	C_1	τ_{a2} (s)	C_2	τ_d (s)
20 nM	0.31±0.06	0.48±0.03	2.95±0.32	0.52±0.03	1.28±0.11
2 μM	0.45±0.07	0.54±0.07	5.48±0.92*	0.46±0.07	0.78±0.09*

The data were derived from records gained at V_m=±50 mV. τ_{a1}, τ_{a2}: time constants of I_{hc} activation of the fast and slow component, i.e., I_{hc1} and I_{hc2}. C_1, C_2: relative contribution of I_{hc1} and I_{hc2} corresponding to the fractional amplitude of I_{hc} at steady state. τ_d: time constant of I_{hc} deactivation. Number of experiments at $[Ca^{2+}]_o$=20 nM: n=10 (τ_{a1}, τ_{a2}), n=16 (τ_d); at $[Ca^{2+}]_o$=2 μM: n=6 (τ_{a1}, τ_{a2}), n=9 (τ_d)

*Significant at p<0.01. For explanations, see text

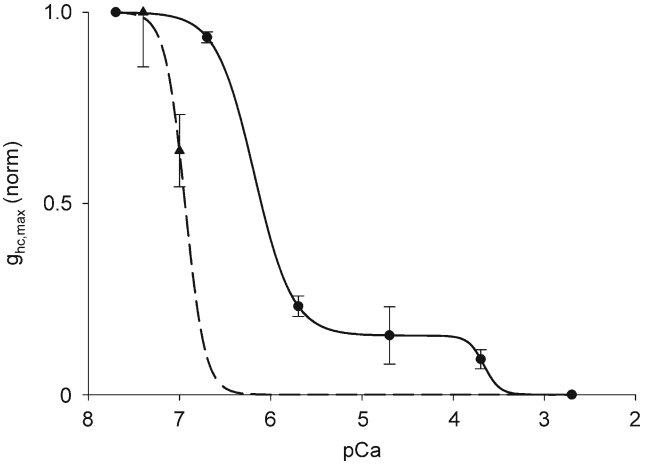

Fig. 3 Dose–response relationship between $g_{hc,max}$ and $[Ca^{2+}]_o$. The values of $g_{hc,max}$ were obtained at different $[Ca^{2+}]_o$. For each $[Ca^{2+}]_o$ tested, the amplitude of I_{hc} was determined at the end of the conditioning pulse at quasi-steady-state condition, $I_{hc,max}$, and the conductance $g_{hc,max}$ calculated (V_m=50 mV). The normalized values of $g_{hc,max}$ were plotted as a function of the negative logarithm of $[Ca^{2+}]_o$ (*filled circles*). The solid curve represents the best fit of data to a Hill equation (for values, see text). For comparison, the graph also presents the dose–response relationship between $g_{hc,max}$ and $[Ca^{2+}]_i$ (*filled triangles*, dashed curve; for values, see text)

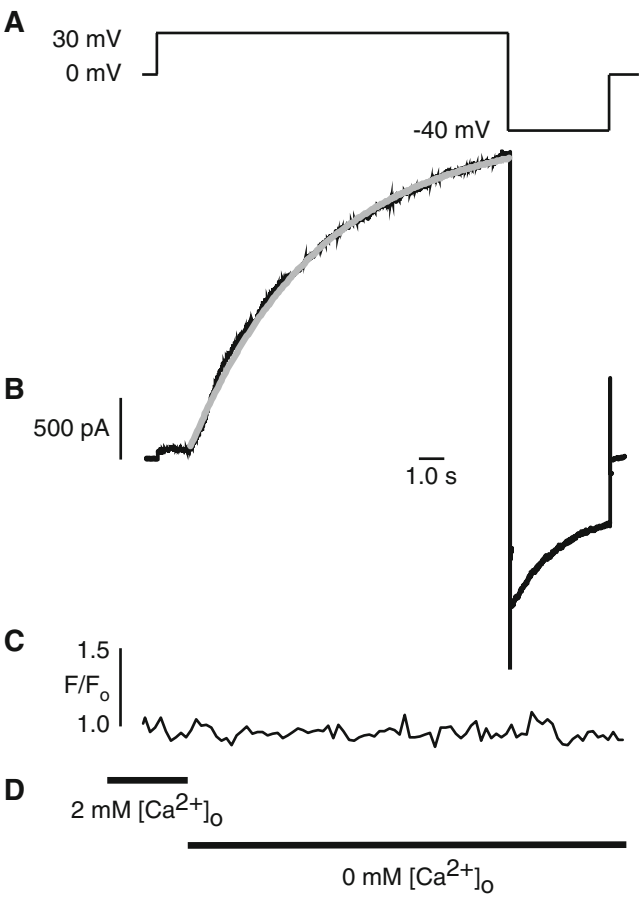

Fig. 4 Response time of I_{hc} to rapid changes in $[Ca^{2+}]_o$. **a** Voltage protocol. Conditioning pulse to 30 mV followed by a test pulse to −40 mV. Note different protocol (see Fig. 1). **b** I_{hc} signal. **d** Extracellular solution change. **c** Time course of fluo-3 fluorescence recorded under the whole-cell configuration of the voltage-clamp technique; the rapid ($t_{1/2}$≈400 ms) change in $[Ca^{2+}]_o$ was induced by fast superfusion and led to instantaneous activation of I_{hc} with a τ of 3.8±0.4 ms (n=5). **d** Extracellular solution change. This intervention was not accompanied by changes in $[Ca^{2+}]_i$ whatsoever. The time course was fitted by using an exponential function, means ±1 SEM

with the solution change (compare traces B and D). Prior to solution change, i.e., in the presence of 2 mM $[Ca^{2+}]_o$ (trace D), the conditioning pulse was accompanied by a negligible outward current (trace B). It resembles the current during maintained superfusion with 2 mM Ca^{2+} solution and reflects unspecific background and/or leak current evoked by the conditioning pulse. Simultaneous measurement of the intracellular Ca^{2+} by means of fluo-3 and confocal microscopy yielded no change in free $[Ca^{2+}]_i$ when $[Ca^{2+}]_o$ was reduced (trace C). Similar results were obtained in five other cells. Please note that the electrical/optical studies used V_m steps of 30/−40 mV instead of 50/−50 mV (compare Fig. 1 with Figs. 4 and 5). This more gentle protocol ensured less stress on cells.

Rapid superfusion experiments were also carried out with external solutions containing 50, 100, 150, and 200 nM Ca^{2+} (data not shown). Results showed that the larger the level of $[Ca^{2+}]_o$, the slower was the time-dependent activation of I_{hc} and the smaller the amplitude of I_{hc} at steady state reached and vice versa. There was no sign of a change in $[Ca^{2+}]_i$, irrespective of the prevailing $[Ca^{2+}]_o$. The current traces in Fig. 1 already alluded to this behavior.

Effects of intracellular Ca^{2+} on hemichannel currents

An attempt was also made to study the effects of intracellular Ca^{2+} on I_{hc}. Cells were dialyzed with pipette solution containing different Ca^{2+} concentrations and the dual-pulse protocol was used to elicit I_{hc} (conditioning pulse=30 mV, 10 s; test pulse=−40 mV, 5 s). Prior to measurements, the cells were superfused with solution containing 20 nM Ca^{2+} to avoid interference from extracellular Ca^{2+}. Two to three minutes after disruption of the membrane patch, the ionic content of the cytosol reached equilibrium as evident from stable current recordings. I_{hc} signals were then gathered to measure $I_{hc,max}$ and calculate $g_{hc,max}$. The values obtained from individual cells were sampled and averaged to determine the mean values at different $[Ca^{2+}]_i$. Reliable data were obtained over a limited range of $[Ca^{2+}]_i$, i.e., 40 nM ($g_{hc,max}$=25.4±2.4 μS; n=8) and 100 nM ($g_{hc,max}$=16.2±2.3 μS; n=7). Measurements at larger $[Ca^{2+}]_i$ were difficult to carry out and interpret because of deleterious effects on cells.

Figure 3 also depicts the concentration–response relationship of the function $g_{hc,max}=f([Ca^{2+}]_i$ (filled triangles,

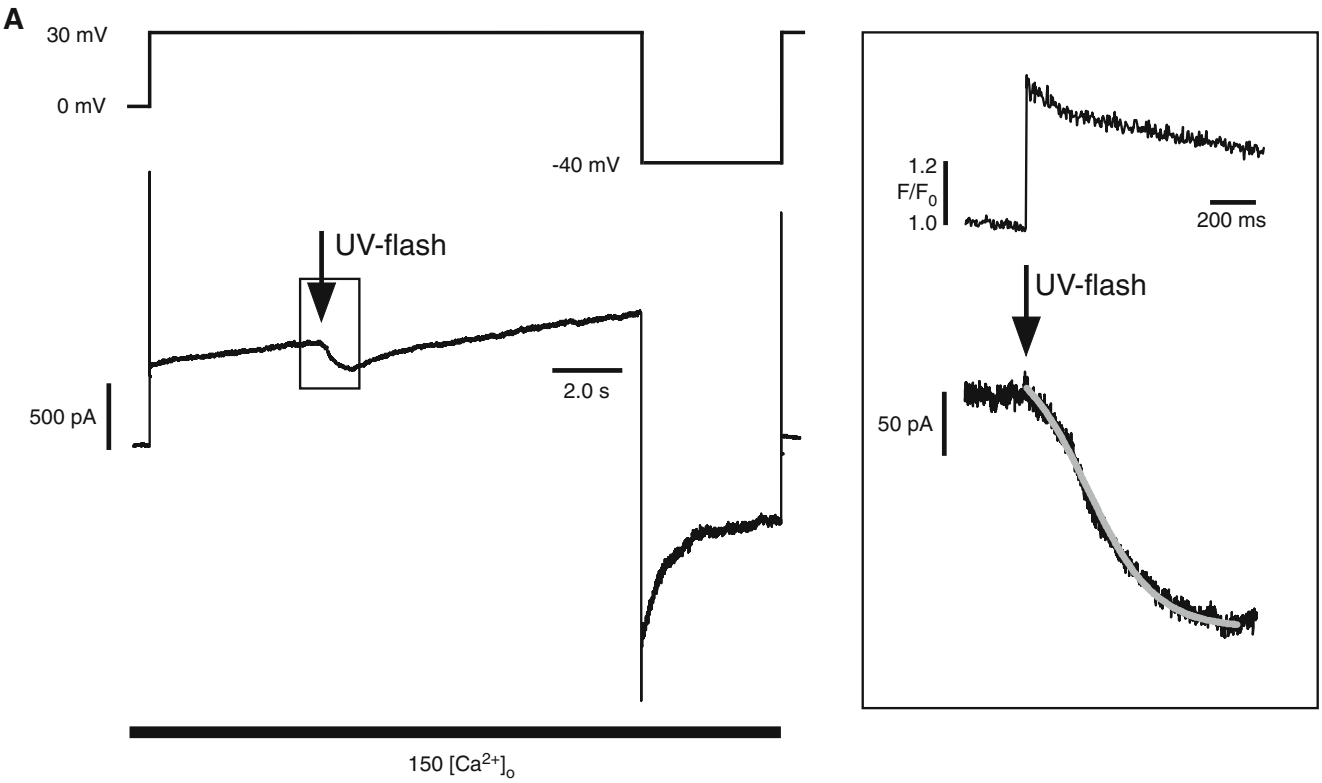

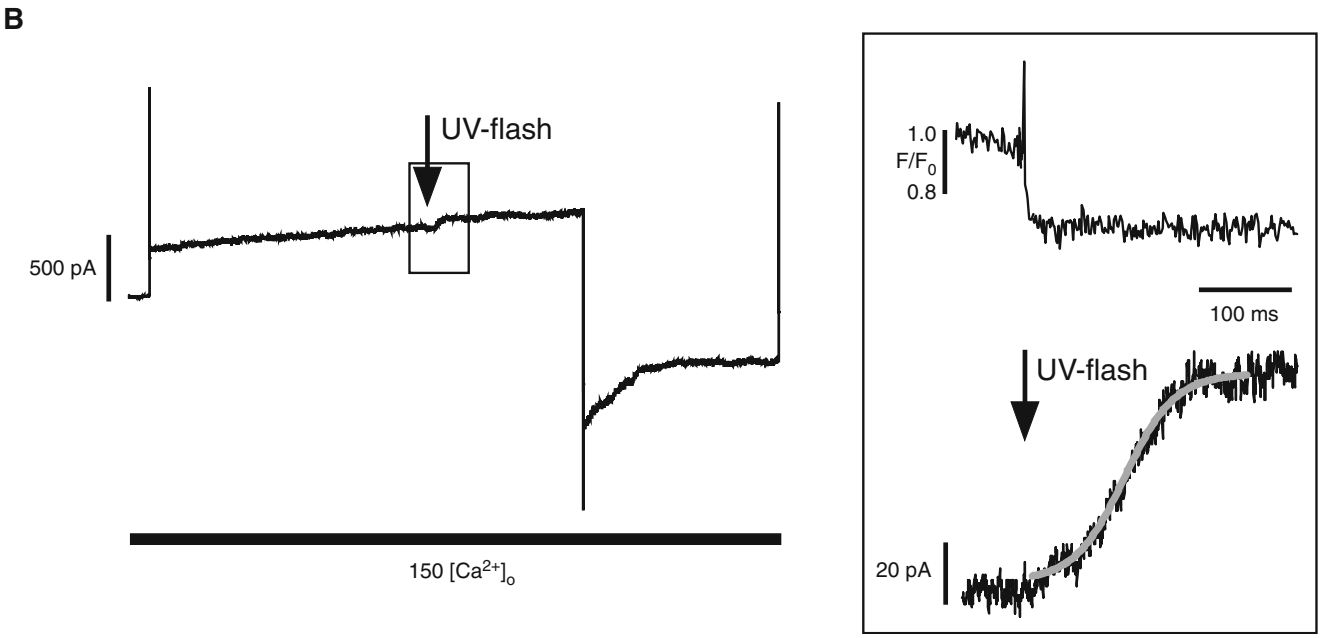

Fig. 5 **a**, **b** Response time of I_{hc} to rapid changes in $[Ca^{2+}]_i$. Rapid changes of $[Ca^{2+}]_i$ (resting $[Ca^{2+}]_i$=100 nM) were induced by UV-flash photolysis of caged Ca^{2+} (DM-nitrophen) and the photoactivatable Ca^{2+} scavenger (diazo-2) under whole-cell configuration of the voltage-clamp technique. **a** *Top*: voltage protocol. A conditioning voltage pulse to 30 mV was followed by a test pulse to −40 mV in $[Ca^{2+}]_o$=150 nM (*bottom*). Note different protocol (see Fig. 1). *Middle*: I_{hc} signal. The inset (*right-hand side*) at expanded time scale shows the fluo-3 fluorescence change measured in line-scan mode after photorelease of Ca^{2+} and the corresponding I_{hc} response. Rapid increase in $[Ca^{2+}]_i$ due to uncaging of DM-nitrophen inhibited I_{hc} with a time constant (τ) of 246±61 ms (n=5). **b** I_{hc} was activated under similar conditions (see (**a**)). The inset (*right-hand side*) at expanded time scale shows the decrease in fluo-3 fluorescence after photorelease of the "caged" Ca^{2+} chelator, diazo-2, and the corresponding I_{hc} response. Flash photolysis of diazo-2 rapidly and homogeneously decreased $[Ca^{2+}]_i$ and the corresponding I_{hc} increased simultaneously with a time constant (τ) of 272±109 ms (n=5). The time course was fitted by using a sigmoidal function, means ±1 SEM

dashed curve). The symbols represent means ±1 SEM. Mean values of $g_{hc,max}$ were normalized and plotted as a function of pCa_i. The plot was obtained by setting the average $g_{hc,max}$ in $[Ca^{2+}]_i$=20 nM to unity and scale the data for $[Ca^{2+}]_i$=40 nM and 100 nM accordingly. Fitting the available data to a single Hill equation (see Eq. 2) yielded the following values: pK'_{Ca}=6.94 (apparent binding constant, corresponding to K_{Ca}=0.12 μM; n=4); places a lower limit of four binding sites for Ca^{2+} per HC.

Response time of hemichannel currents to rapid changes in $[Ca^{2+}]_i$

A set of experiments was performed to assess the response time of I_{hc} to sudden changes in intracellular Ca^{2+}. Step increases of $[Ca^{2+}]_i$ were induced by means of UV-flash photolysis of caged Ca^{2+}. Figure 5 illustrates the result of an experiment carried out under following conditions. $[Ca^{2+}]_i$ was set to 100 nM and $[Ca^{2+}]_o$ to 150 nM using EGTA buffer. Interference from Na^+/Ca^{2+} exchange was minimized by adding 1 mM Ni^{2+} to the bath solution in some experiments. Moreover, the Ca^{2+} pump of the endoplasmic reticulum was blocked by 0.1 μM thapsigargin added to the pipette solution. Both precautions prevented the removal of Ca^{2+} from the cytoplasm during subsequent interventions. I_{hc} was elicited with a bipolar voltage pulse. Figure 5, left-hand panel, shows the pulse protocol (upper trace) and the I_{hc} signal (lower trace). Depolarization to 30 mV for 15 s gave rise to a gradual increase in outward current. During the development of the current, a UV flash was applied (inset with arrow). This resulted in a distinct transient decrease in I_{hc}. Figure 5a, right-hand panel, repeats the current trace at higher resolution (lower signal). I_{hc} began to decrease at the incidence of flashing (see arrow) and then developed in a sigmoidal fashion. The maximal response was reached within 1 s. The decrease in I_{hc} developed more rapidly than the recovery. Figure 5a, right-hand panel, also shows the simultaneous measurement of $[Ca^{2+}]_i$ by means of confocal microscopy and fluo-3 in the pipette solution (upper signal). The trace displays the $[Ca^{2+}]_i$ versus time after the flash. It shows that $[Ca^{2+}]_i$ increased in milliseconds. The free intracellular Ca^{2+} recovered within 5 s (signal truncated). The recovery occurred in two phases, an exponential phase followed by a linear one. Signal calibration yielded an initial change in Ca^{2+} of about 400 nM. The line scan of the Ca^{2+} signal documented the homogeneity of the Ca^{2+} signal (not shown). The time constant, τ, of $[Ca^{2+}]_o$ change was 246±61 ms (n=7).

Step decreases of $[Ca^{2+}]_i$ were induced by means of UV-flash activation of a Ca^{2+} scavenger, diazo-2 (Fig. 5b). The experiments were performed under the same conditions as the previous ones. The left-hand panel shows the I_{hc} signal. The inset with the arrow marks the incidence of flashing. Figure 5b, right-hand panel, repeats the I_{hc} signal at higher resolution (lower trace) and the fluorescence $[Ca^{2+}]_i$ signal (upper trace). The arrow marks the incidence of flashing. The intervention provoked a decrease of about ≈25–50 % in $[Ca^{2+}]_i$ associated with a sigmoidal increase in I_{hc}. On average, the time constant, τ, of the change in $[Ca^{2+}]_i$ was 272±109 ms (n=7).

Discussion

In single HCs, two intrinsic gating mechanisms characterized by fast transitions (<1 ms, fast V_m gating) between the main state and the residual state, and slow transitions (>5 ms, slow V_m gating) between an open state and the closed state have been identified [37]. The fast gate seems to reside at the cytoplasmic end of a HC and to involve the C-terminal domain of Cxs [6], and the slow gate at the extracellular end and to involve the extracellular loops E1 and E2 [19, 23, 42]. The fast gate responds to negative or positive voltage, depending on the type of Cx; the slow gate always to negative voltage [6] and is modulated by divalent cations, primarily Ca^{2+} [10, 23, 37, 41]. In Cx45 HCs, both gates close at negative V_m [4]. Since both are arranged in series, V_m acts on both gates in a competitive manner, i.e., closure of one gate entails a collapse of V_m across this very gate and reduces V_m across the other gate and vice versa. Hence, the open probability of a gate depends on the state of the other gate via changes in the local electric field, leading to contingent gating [18, 22, 43].

The regulatory functions of Ca^{2+} on GJC and HCs are still enigmatic and experimental observations are contradictory. The present study examined in detail the effects of extra- and intracellular $[Ca^{2+}]$ on the properties of I_{hc} under two different experimental conditions.

Extracellular calcium

Steady-state properties of I_{hc}

Previous studies have reported conflicting data on $[Ca^{2+}]_o$ regulation and corresponding voltage shifts of $g_{hc,ss} = f(V_m)$ on I_{hc}. Elevation of $[Ca^{2+}]_o$ provokes a large shift (tens of millivolts) to more positive voltage in Cx46 [10, 11, 23, 41], a small shift (few millivolts) in Cx32 and Cx35 [15, 40], and no shift in Cx37 and Cx50 [3, 24]. Conceivably, the data variance reflects an intrinsic property of Cxs. Interestingly, despite a structural identity of 33 %, the functional properties of Cx45 and Cx46 are different. Furthermore, we found that elevation of $[Ca^{2+}]_o$ decreased $I_{hc,max}$, decelerated the rate of I_{hc} activation, and accelerated the rate of I_{hc} deactivation of Cx45 HCs reversibly upon return to 20 nM (Fig. 2a). The larger $[Ca^{2+}]_o$, the smaller was the amplitude

of $g_{hc,ss}$ at a given V_m. In addition, Cx45 HCs show no sign of a surface charge effect by external Ca^{2+}.

At large positive V_m, $g_{hc,ss}$ approaches a maximum, $g_{hc,max}$, which corresponds to an endpoint of $g_{hc,ss} = f(V_m)$ for each $[Ca^{2+}]_o$. Accordingly, $g_{hc,max}$ reflects the number of HCs dwelling in the main state, unaffected by V_m-dependent fast and slow gating. As to the effects of $[Ca^{2+}]_o$, $g_{hc,max}$ represents the ratio of HCs in the main state versus closed state, controlled by interaction of external Ca^{2+} with slow V_m gating. The lower the level of $[Ca^{2+}]_o$, the larger the number of HCs in the main state and vice versa. At large negative V_m, $g_{hc,ss}$ approaches a minimum, $g_{hc,min}$, which corresponds to the number of HCs in the residual state and main state set by fast and slow V_m gating, respectively, acting in a contingent manner. This behavior is consistent with the view that external Ca^{2+} modifies HC properties through reversible binding to regulatory sites located in the channel lumen and/or its outer vestibule, thus affecting voltage sensors and blocking/unblocking the pore [10, 15, 23, 35, 42].

Interestingly, $g_{hc,min}$ did not decline to zero, even at the lowest $[Ca^{2+}]_o$ tested (Table 1, Fig. 2a). This implies that V_m-sensitive gating is intrinsic to Cx45 HCs and requires no external Ca^{2+} and is in agreement with the finding that P_o of Cx45 HCs under Ca^{2+}-free solution does not reach zero at large negative V_m [39]. In contrast, Cx46 and Cx37 HCs appears to fail V_m gating in low $[Ca^{2+}]_o$ [10, 24]. However, this interpretation has been recently challenged [41].

Kinetics of I_{hc}

V_m depolarization evoked an outward current with two components, a sudden rise, $I_{hc,inst}$, reflecting the functional state of HCs prior to depolarization, i.e., V_h=0 mV, and a subsequent time-dependent increase representing I_{hc} activation; V_m hyperpolarization led to an inward current with a time-dependent decrease documenting I_{hc} deactivation, both governed by V_m gating. These results gained in 20 nM and 2 μM $[Ca^{2+}]_o$ concur with data previously reported for Cx45 in $[Ca^{2+}]_o \cong 10$ nM [1]. Analysis of I_{hc} in the presence of low and high $[Ca^{2+}]_o$ revealed two processes of activation (I_{hc1}, I_{hc2}) and a single process of deactivation, giving rise to two time constants of activation, τ_{a1} and τ_{a2}, and a single one of deactivation, τ_d (see Table 2). The former may reflect fast and slow V_m gating during depolarization, the latter V_m gating during hyperpolarization. Not unrealistically, we assume the existence of two time constants of deactivation, τ_{d1} and τ_{d2}, whose values are too similar to be resolved. Table 2 shows that $\tau_{a1} < \tau_{a2}$, $\tau_{a1} < \tau_d$, and $\tau_{a2} > \tau_d$, irrespective of $[Ca^{2+}]_o$. Moreover, it indicates that elevation of $[Ca^{2+}]_o$ led to a significant increase of τ_{a2} and decrease of τ_d, while τ_{a1}, C_1, and C_2 remained virtually unchanged. Furthermore, it caused $I_{hc,inst}$ to decrease (Fig. 1). Hence, $[Ca^{2+}]_o$ does not only modulate kinetics of slow V_m gating (i.e., τ_{a2} and τ_d), it also sets the number of open HCs, $I_{hc,inst}$ (see above). As in Cx45 HCs, elevation of $[Ca^{2+}]_o$ decelerates activation and accelerates deactivation in Cx46 [11]. However, it accelerates activation and deactivation in Cx32 [15], and accelerates deactivation in Cx37 [24], but has no effect in Cx50 [3] indicating that kinetic properties also depend on the type of HC.

Relationship between $[Ca^{2+}]_o$ and g_{hc}

The shape of the normalized curve $g_{hc,max} = f([Ca^{2+}]_o)$ (Fig. 3) suggests the presence of two different regulatory Ca^{2+}-binding sites enabling reversible HC block: (1) high-affinity binding and low $[Ca^{2+}]_o$, and (2) low-affinity binding and high $[Ca^{2+}]_o$. Since there is no overlap, the two regulatory systems act sequentially. Ca^{2+} is likely to interfere with cationic binding sites putatively located in the lumen of a channel and/or its vestibule. For convenience, it might be useful to define a $[Ca^{2+}]_o$ threshold for chemical gating. Consider the value of $[Ca^{2+}]_o$ at $g_{hc,max}(norm)$= 0.025 for process 2, the threshold would be 440 μM. However, this $[Ca^{2+}]_o$ would be close to physiological settings. Based on Hill parameters reported for HCs, the sensitivity to external Ca^{2+} seems to be Cx specific, Cx45 being most sensitive and Cx32 least [3, 15, 24, 36].

Rapid changes in $[Ca^{2+}]_o$

The rapid modulatory effect of $[Ca^{2+}]_o$ on I_{hc} in response to rapid external solution change is consistent with a direct action of extracellular Ca^{2+} on HCs ($g_{hc,max}$) rather than an effect mediated by molecular intermediates, e.g., calmodulin [20]. Comparison of Figs. 4 and 1 reveals that step changes in $[Ca^{2+}]_o$ and V_m generate I_{hc} signals of different contour. The rapid rise in outward I_{hc} was absent and the subsequent time-dependent outward I_{hc} developed as single exponential instead of a dual exponential. Moreover, its time course was decelerated. Thus, V_m gating proceeds faster than Ca^{2+} gating, a process driven by external Ca^{2+} named chemical gating. Conceivably, Ca^{2+} act on receptor sites located in the channel lumen and/or its outer mouth provoking block/unblock, thus setting the number of HCs available for V_m gating. Concomitant measurement of free $[Ca^{2+}]_i$ revealed that changes in $[Ca^{2+}]_o$ did not alter internal Ca^{2+} (Fig. 4c), implying that chemical gating is solely controlled by external Ca^{2+}. This is consistent with the view that cytosolic intermediates are not involved in Ca^{2+} gating. At 30 mV, most HCs were closed due to block by high external Ca^{2+}. Subsequent rapid lowering of $[Ca^{2+}]_o$ to 20 nM initiated unblock of HCs and led to a growing number of open channels, thus giving rise to a time-dependent increase in I_{hc} aiming for a steady state. The rise in I_{hc} developed more slowly when

evoked by a step change in $[Ca^{2+}]_o$ than a step change in V_m (Figs. 4 and 1). This reflects a difference in the nature of the underlying processes, i.e., Ca^{2+} gating driven by concentration gradient versus V_m gating driven by voltage gradient. However, an effect of external Ca^{2+} on V_m gating cannot be excluded.

Intracellular calcium

Relationship between $[Ca^{2+}]_i$ and g_{hc}

Efforts to determine the curve $g_{hc,max} = f([Ca^{2+}]_i)$ were successful. However, data analysis yielded a system with high-affinity binding and relatively low $[Ca^{2+}]_o$. A comparison of $g_{hc,max} = f([Ca^{2+}]_i)$ (Fig. 3, dashed curve) and $g_{hc,max} = f([Ca^{2+}]_o)$ (Fig. 3, solid curve) reveals that Cx45 HCs are more sensitive to $[Ca^{2+}]_i$ than $[Ca^{2+}]_o$. This may imply two locations of Ca^{2+}-binding sites, one putatively at the outer face of a channel responding to $[Ca^{2+}]_o$ and one at the inner face reacting to $[Ca^{2+}]_i$. However, this interpretation has to be further examined. Interestingly, exposure of Cx46 HCs to high Ca^{2+} on either side leads to robust channel closure [23]. Hence, the authors postulated a single gate localized extracellular to position 35. Moreover, earlier studies on cardiomyocytes expressing predominantly Cx43 were devoted to the sensitivity of GJCs to internal Ca^{2+}. They yielded a broad range of Hill parameters (pK'_{Ca}=6.4, K_{Ca}=0.40 μM; n=3.6, [21]; pK'_{Ca}=3.5, K_{Ca}=315 μM, n=0.87, [13]).

Rapid changes in $[Ca^{2+}]_i$

Rapid increase in $[Ca^{2+}]_i$ induced by photorelease of caged Ca^{2+} elicited a rapid onset (milliseconds) of inward I_{hc} that evolved into a sigmoidal decay (Fig. 5a). Conversely, a decrease in $[Ca^{2+}]_i$ caused by Ca^{2+} binding to a scavenger initiated a rapid onset (milliseconds) of outward I_{hc} developing into a sigmoidal rise (Fig. 5b). The latter response was less prominent due to cytosolic redistribution of Ca^{2+} via diffusion. The quasi-instantaneous response indicates that I_{hc} is directly controlled by internal Ca^{2+} and argues against indirect effects by biochemical intermediates [20]. Again, it supports the concept that Cx45 HCs have separate Ca^{2+}-binding sites located at the outer and inner face of channels. Conceivably, Cx45 HCs are also regulated by binding of internal Ca^{2+} to sites located near the cytosolic face of HCs, thus altering channel properties.

Relevance of data

Cx45 HCs have a sizable conductance and permeability [39] and should therefore be closed under physiological conditions. This is essential to maintain ionic gradients and cytosolic concentrations. According to Fig. 3, the low-affinity Ca^{2+}-binding system operates close to the range of $[Ca^{2+}]_o$ relevant to regulate the open/closed state of Cx45 HCs under physiological conditions, i.e., 2 mM. An estimate of its threshold level is ~440 μM (see above). Given the channel conductance, few open HCs would be necessary to exert a prominent effect. It is possible that unapposed HCs are involved in regulating cell–cell interactions. Conceivably, Ca^{2+} gating may play a role during HC docking. The functional relevance of such a regulatory system has to be validated. However, pathophysiological situations in cardiac tissue are associated with complex changes in the Ca^{2+} signaling and remodeling of regional gradients in expression of connexins. Thus, regulatory functions of Ca^{2+} on GJC may contribute to cardiac electrical dysfunction and arrhythmias. However, be aware, all experiments have been carried out at room temperature, not at body temperature (the relevant temperature coefficients are physical—Q_{10} ~1; chemical—Q_{10} ~2; biochemical—Q_{10} up to ~4).

We demonstrate that Ca^{2+} regulation of Cx45 HCs occurs too quick to be mediated by biomolecular intermediates, such as calmodulin. Interestingly, a previous study reported that Ca^{2+}-dependent inhibition of Cx43 GJs is mediated by calmodulin binding to the intracellular loop region of Cx43 [47]. Moreover, the combination of electrical and optical methods turned out to be promising in HC research. In the present paper, we succeeded to differentiate between current driven by concentration gradient and current driven by voltage gradient.

Acknowledgments We thank Daniel Lüthi for technical assistance and S. Cohen for helpful comments on the manuscript. This work was supported by the Swiss National Science Foundation (31-111983 to M.E., 31-67230.01 and 31-108175.05 to R.W.).

References

1. Bader P, Weingart R (2004) Conductive and kinetic properties of connexin45 hemichannels expressed in transfected HeLa cells. J Membr Biol 199:143–154
2. Bader P, Weingart R (2006) Pitfalls when examining gap junction hemichannels: interference from volume-regulated anion channels. Pflügers Arch 453:396–406
3. Beahm DL, Hall JE (2002) Hemichannel and junctional properties of connexin 50. Biophys J 82:2016–2031
4. Bukauskas FF, Bukauskiene A, Verselis VK, Bennett MVL (2002) Coupling asymmetry of heterotypic connexin 45/connexin 43-EGFP gap junctions: properties of fast and slow gating mechanisms. PNAS (USA) 99:7113–7118
5. Bukauskas FF, Elfgang C, Willecke K, Weingart R (1995) Biophysical properties of gap junction channels formed by mouse connexin40 in induced pairs of transfected human HeLa cells. Biophys J 68:2289–2298
6. Bukauskas FF, Verselis VK (2004) Gap junction channel gating. Biochim Biophys Acta 1662:42–60

7. Butterweck A, Gergs U, Elfgang C, Willecke K, Traub O (1994) Immunochemical characterization of the gap junction protein connexin45 in mouse kidney and transfected human HeLa cells. J Membr Biol 141:247–256
8. Délèze J (1970) The recovery of resting potential and input resistance in sheep heart injured by knife of laser. J Physiol 208:547–562
9. Derouette J-P, Desplantez T, Wong CW, Roth I, Kwak BR, Weingart R (2009) Functional differences between human Cx37 polymorphic hemichannels. J Mol Cell Cardiol 46:499–507
10. Ebihara L, Liu X, Pal JD (2003) Effect of external magnesium and calcium on human connexin46 hemichannels. Biophys J 84:277–286
11. Ebihara L, Steiner E (1993) Properties of a nonjunctional current expressed from a rat connexin46 cDNA in *Xenopus* oocytes. J Gen Physiol 102:59–74
12. Elfgang C, Eckert R, Lichtenberg-Fraté H, Butterweck A, Traub O, Klein RA, Hülser DF, Willecke K (1995) Specific permeability and selective formation of gap junction channels in connexin-transfected HeLa cells. J Cell Biol 129:805–817
13. Firek L, Weingart R (1995) Modification of gap junction conductance by divalent cations and protons in neonatal rat heart cells. J Mol Cell Cardiol 27:1633–1643
14. Gomes P, Srinivas SP, Vereecke J, Himpens B (2006) Gap junctional intercellular communication in bovine corneal endothelial cells. Exp Eye Res 83:1225–1237
15. Gómez-Hernández JM, de Miguel M, Larrosa B, Gonzáles D, Barrio LC (2003) Molecular basis of calcium regulation in connexin-32 hemichannels. Proc Natl Acad Sci U S A 100:16030–16035
16. Haefliger JA, Nicod P, Meda P (2004) Contribution of connexins to the function of the vascular wall. Cardiovasc Res 62:345–356
17. Harris AL (2001) Emerging issues of connexin channels: biophysics fills the gap. Quart Rev Biophys 34:325–472
18. Harris AL, Spray DC, Bennett MVL (1981) Kinetic properties of a voltage-dependent junctional conductance. J Gen Physiol 77:95–117
19. Kronengold J, Trexler EB, Bukauskas FF, Bargiello TA, Verselis VK (2003) Single-channel SCAM identifies pore-lining residues in the first extracellular loop and first transmembrane domains of Cx46 hemichannels. J Gen Physiol 122:389–405
20. Lurtz MM, Louis CF (2003) Intracellular calcium regulation of connexin43. Am J Physiol Cell Physiol 293:C1806–C1813
21. Noma A, Tsuboi N (1987) Dependence of junctional conductance on proton, calcium and magnesium in cardiac paired cells of guinea-pig. J Physiol 382:193–211
22. Paullauskas N, Pranevicius M, Pranevicius H, Bukauskas FF (2009) A stochastic four-state model of contingent gating of gap junction channels containing two 'fast' gates sensitive to transjunctional voltage. Biophys J 96:3936–3948
23. Pfahnl A, Dahl G (1999) Gating of Cx46 gap junction hemichannels by calcium and voltage. Pflügers Arch 437:345–353
24. Puljung MC, Berthoud VM, Beyer EC, Hanck DA (2004) Polyvalent cations constitute the voltage gating particle in human connexin37 hemichannels. J Gen Physiol 124:587–603
25. Rose B, Loewenstein WR (1975) Permeability of cell junction depends on local cytoplasmic calcium activity. Nature 254:250–252
26. Rozental R, Srinivas M, Gokhan S, Urban M, Dermietzel R, Kessler JA, Spray DC, Mehler MF (2000) Temporal expression of neuronal connexins during hippocampal ontogeny. Brain Res Brain Res Rev 32:57–71
27. Sáez JC, Connor JA, Spray DC, Bennett MVL (1989) Hepatocyte gap junctions are permeable to the second messenger, inositol 1,4,5-trisphosphate, and the calcium ion. Proc Natl Acad Sci U S A 86:2708–2712
28. Sáez JC, Retamal MA, Basilio D, Bukauskas FF, Bennett MVL (2005) Connexin-based gap junction hemichannels: gating mechanisms. Biochim Biophys Acta 1711:215–224
29. Scemes E, Giaume C (2006) Astrocyte calcium waves: what they are and what they do. Glia 54:716–725
30. Severs NJ, Coppen SR, Dupont E, Yeh HI, Ko YS, Matsushita T (2004) Gap junction alterations in human cardiac disease. Cardiovasc Res 62:368–377
31. Sohl G, Guldenagel M, Traub O, Willecke K (2000) Connexin expression in the retina. Brain Res Brain Res Rev 32:138–145
32. Spray DC, Stern JH, Harris AL, Bennett MVL (1982) Gap junction conductance: comparison of sensitivities to H and Ca ions. Proc Natl Acad Sci U S A 79:441–445
33. Spray DC, Ye Z-C, Ransom BR (2006) Functional connexin "hemichannels": a critical appraisal. Glia 64:758–773
34. Stout CE, Costantin JL, Naus CCG, Charles AC (2002) Intercellular calcium signaling in astrocytes via ATP release through connexin hemichannels. J Biol Chem 277:10482–10488
35. Thimm J, Mechler A, Lin H, Rhee S, Lal R (2005) Calcium-dependent open/closed conformations and interfacial energy maps of reconstituted hemichannels. J Biol Chem 280:10646
36. Tong J-J, Ebihara L (2006) Structural determinants for the differences in voltage gating of chicken Cx56 and Cx45.6 gap-junctional hemichannels. Biophys J 91:2142–2154
37. Trexler EB, Bennett MVL, Bargiello TA, Verselis VK (1996) Voltage gating and permeation in a gap junction hemichannel. Proc Natl Acad Sci U S A 93:5836–5841
38. Trexler EB, Bukauskas FF, Kronengold J, Bargiello TA, Verselis VK (2000) The first extracellular loop domain is a major determinant of charge selectivity in connexin46 channels. Biophys J 79:3036–3051
39. Valiunas V (2002) Biophysical properties of connexion-45 gap junction hemichannels studied in vertebrate cells. J Gen Physiol 119:147–164
40. Valiunas V, Mui R, McLachlan E, Valdimarsson G, Brink PR, White TW (2004) Biophysical characterization of zebrafish connexin35 hemichannels. Am J Physiol Cell Physiol 287:C1596–C1604
41. Verselis VK, Srinivas M (2008) Divalent cations regulate connexin hemichannels by modulating intrinsic voltage-dependent gating. J Gen Physiol 132:315–327
42. Verselis VK, Trelles MP, Rubinos C, Bargiello TA, Srinivas M (2009) Loop gating of connexin hemichannels involves movement of pore-lining residues in the first extracellular loop domain. J Biol Chem 284:4484–4493
43. Vogel R, Weingart R (1998) Mathematical model of vertebrate gap junctions derived from electrical measurements on homotypic and heterotypic channels. J Physiol 510(1):177–189
44. Warn-Cramer BJ, Lau AF (2004) Regulation of gap junctions by tyrosine protein kinases. Biochim Biophys Acta 1662:81–95
45. Weingart R (1977) The actions of ouabain on intercellular coupling and conduction velocity in mammalian ventricular muscle. J Physiol 264:341–365
46. Wong CW, Christen T, Roth I, Chadjichristos CE, Derouette J-P, Foglia BF, Chanson M, Goodenough DA, Kwak BR (2006) Connexin37 protects against atherosclerosis by regulating monocyte adhesion. Nat Med 12:950–954
47. Zhou Y, Yang W, Lurtz MM, Ye Y, Huang Y, Lee H-W, Chen Y, Louis CF, Yang JJ (2007) Identification of the calmodulin binding domain of connexin 43. J Biol Chem 282:35005–350017